Comparison of GEOS-Chem aerosol optical depth with AERONET and MISR data over the contiguous United States

Shenshen Li,[1,2] Michael J. Garay,[3] Liangfu Chen,[1] Erika Rees,[2] and Yang Liu[2]

Received 8 April 2013; revised 24 September 2013; accepted 25 September 2013; published 10 October 2013.

[1] Aerosol optical properties simulated by the global 3-D tropospheric chemistry and transport model Goddard Earth Observing System (GEOS)-Chem (GC) from 2008 to 2010 over the contiguous United States were evaluated with ground observations from Aerosol Robotic Network (AERONET) sites and aerosol products reported by the Multiangle Imaging Spectroradiometer (MISR). Overall, the correlation coefficient (r) and regression slope between AERONET and $GC_{2^\circ \times 2.5^\circ}$ (2° latitude × 2.5° longitude) daily total column aerosol optical depth (AOD) were 0.6 and 0.51, respectively. After using the nested $GC_{0.5^\circ \times 0.667^\circ}$ model to control for spatial variability, removing several outliers, and averaging over a monthly timescale, the agreement was significantly improved to an r of 0.84 and a slope of 0.75. Seasonal, hourly, and geographical statistics for $GC_{0.5^\circ \times 0.667^\circ}$ and AERONET AODs show a similar data range and variation, with higher mean values in the summer, the evening, and in the eastern U.S. Smaller correlation coefficients are seen in the summer and winter, in the evening, and in the western U.S. To investigate the optical properties of major GC tracers, MISR level 2 aerosol products were used to calculate inorganic aerosol, dust, and absorbing non-dust AOD. Both GC and MISR suggest that on average, inorganic aerosol has the highest AOD (GC: 0.071, MISR: 0.089) nationally, followed by absorbing non-dust species (GC: 0.025, MISR: 0.041), and dust (GC: 0.013, MISR: 0.014). The large discrepancies in our intercomparison are due to GC underestimation of inorganic aerosol levels during all four seasons in the western U.S. and dust during summer in the eastern U.S., along with overestimation of summertime-absorbing non-dust species over the northwestern U.S. These uncertainties are attributed to underestimation of inorganic aerosol emissions in more polluted western regions, the transport of Sahara dust in the summer, misuse of the fire files, MISR retrieval uncertainties in the surface, and choice of aerosol models.

Citation: Li, S., M. J. Garay, L. Chen, E. Rees, and Y. Liu (2013), Comparison of GEOS-Chem aerosol optical depth with AERONET and MISR data over the contiguous United States, *J. Geophys. Res. Atmos.*, *118*, 11,228–11,241, doi:10.1002/jgrd.50867.

1. Introduction

[2] Aerosols, especially those in the accumulation mode (0.1 μm to about 2.5 μm in diameter), are a major air quality concern as they have been associated with a wide range of adverse health effects including asthma attacks, respiratory and cardiovascular diseases, and premature death [*Pope et al*., 2009]. Due to their widespread and significant health impacts, ground level accumulation mode aerosols, also known as fine particulate matter ($PM_{2.5}$, particles with aerodynamic diameters less than 2.5 μm), are considered a criterion of air pollutant and routinely monitored for compliance by a nationwide network operated by the U.S. Environmental Protection Agency and its state and local partners. A recent epidemiological study using historical health records and ground observations in 51 U.S. metropolitan areas showed that a decrease of 10 $\mu g/m^3$ in annual mean $PM_{2.5}$ levels was associated with an estimated increase in mean life expectancy of 0.6 year [*Pope et al*., 2009]. Given its diverse emission profiles and relatively short residence time in the lower troposphere, the spatial distribution of $PM_{2.5}$ is rather heterogeneous. Existing ground-monitoring networks in North America and part of Europe mostly cover urban centers due to high operating and maintenance costs. For the rest of the world, especially in developing countries with heavy air pollution, routine $PM_{2.5}$ monitoring is either very sparse or nonexistent. The lack of comprehensive $PM_{2.5}$ exposure estimates hinders research on its health impacts. During the past decade, researchers have explored the

[1]State Key Laboratory of Remote Sensing Science, Institute of Remote Sensing and Digital Earth, Chinese Academy of Sciences, Beijing, China.
[2]Rollins School of Public Health, Emory University, Atlanta, Georgia, USA.
[3]Jet Propulsion Laboratory, California Institute of Technology, Pasadena, California, USA.

Corresponding author: Y. Liu, Rollins School of Public Health, Emory University, 1518 Clifton Road NE, Atlanta, GA 30322, USA. (yang.liu@emory.edu)

2169-897X/13/10.1002/jgrd.50867

potential of using satellite-retrieved aerosol properties together with atmospheric Chemical Transport Models (CTMs) to fill in the gaps between costly and sparse ground observations [*Liu et al*., 2004b; *van Donkelaar et al*., 2010]. Most recently, using satellite-retrieved aerosol optical depth (AOD) and CTM aerosol simulations, the Global Burden of Disease Study ranked the burden of disease attributable to ambient $PM_{2.5}$ pollution as the ninth highest for both sexes in 2010 among 20 leading risk factors, ahead of other factors such as physical inactivity, diet high in sodium, and high cholesterol [*Lim et al*., 2012].

[3] CTMs have the advantage of being able to provide information on aerosol mass concentration, composition, and optical properties at regional to global scales with complete temporal and spatial coverage. Model simulations have been widely used to characterize aerosols and their impact on climate change and air quality [*Martin et al*., 2010]. However, the accuracy of model simulations depends heavily on the quality of meteorological inputs, atmospheric chemistry schemes, and emission inventories. On the other hand, ground-based observations such as those provided by the Aerosol Robotic Network (AERONET) are often considered as the gold standard for the total column aerosol optical properties, but these point measurements have very limited spatial coverage [*Holben et al*., 1998]. Covering large geographical regions, aerosol products from sensors aboard polar-orbiting satellites provide a limited set of aerosol optical properties but often with higher accuracy at a better spatial resolution than CTM results. Both ground and satellite observations have been used to evaluate the performance of CTMs. For example, *Chin et al*. [2002] compared the AOD results from the Goddard Chemistry Aerosol Radiation and Transport model with the retrievals from the advanced very high resolution radiometer and the Total Ozone Mapping Spectrometer and showed that the model reproduced most of the prominent features of the satellite data, with an overall agreement within a factor of two.

[4] The analysis presented in this paper focuses on the Goddard Earth Observing System (GEOS)-Chem (GC) model, a widely used global, 3-D CTM designed to study tropospheric ozone and related species, aerosols, mercury, carbon, and biogenic gases [*Bey et al*., 2001]. GC can estimate the concentration and optical depth of major $PM_{2.5}$ components including sulfate, nitrate, ammonium, black and organic carbon, dust, and sea salt [*Fairlie et al*., 2007; *Jaegle et al*., 2011; *Park et al*., 2004]. Recently, several studies have used GC-simulated aerosol properties and Moderate Resolution Imaging Spectroradiometer (MODIS) radiances to improve the AOD retrieval [*Drury et al*., 2008; *Wang et al*., 2010]. GEOS-Chem has also been shown to be able to estimate ground level particle concentrations [*van Donkelaar et al*., 2010]. GC-simulated aerosol has been evaluated by surface, aircraft, and satellite data. For example, *Park et al*. [2004] compared the sulfate-nitrate-ammonium aerosol concentrations with observations from surface networks in the U.S. and Europe and with Asian outflow observations from the NASA aircraft mission over the northwest Pacific. *Lin et al*. [2012] used retrievals from the Ozone Monitoring Instrument to constrain emissions of GC NOx and analyzed its uncertainties. *van Donkelaar et al*., [2010] validated the GC aerosol vertical profiles by using observations from the Cloud-Aerosol Lidar and Infrared Pathfinder Satellite Observation (CALIPSO) satellite to estimate the error in satellite-derived $PM_{2.5}$. While previous evaluations of GC aerosol simulations often focused on aerosol concentrations, several intercomparison studies for GC total column AOD were carried out on global scale and source regions [e.g., *Johnson et al*., 2012; *Yu et al*., 2012a], but no studies have specifically focused on comparing speciated optical properties. Here we evaluate the long-term accuracy of GC-simulated aerosol and its speciated AOD over populated areas in the contiguous U.S. under various geographical and climatic conditions. By considering speciated AOD retrievals from Multiangle Imaging Spectroradiometer (MISR), this work extends previous studies by *Drury et al*. [2008], who examined MODIS satellite data in conjunction with airborne and surface data, and *Wang et al*. [2010], who looked specifically at dust. This project has important implications on the applications of GC in air quality and environmental health research.

[5] The rest of the paper is organized such that section 2 describes the various model and satellite data products involved in this analysis and data-processing methods used. Section 3 presents comparison results for various spatial- and temporal-averaging windows and the summary statistics from the different data sets. The agreement in seasonal means, hourly variations, and comparisons of the geographical patterns from GC and AERONET over the contiguous U.S. is shown. Component AODs derived from the MISR product are compared with GC, and the sources of uncertainties are also discussed in detail in this section. Finally, major findings and potential future improvements to the current analysis are summarized in section 4.

2. Data Sets and Data Processing

2.1. GEOS-Chem AOD Simulation

[6] In this study, we use GC version 8.3.2 to simulate tracer optical depths at 3 h temporal resolution, 2° latitude × 2.5° longitude horizontal resolutions, and 37 vertical layers (from the surface up to ~20 km) for the time period from 2008 to 2010. Tracer optical depths in each layer are integrated to yield the total column AOD (τ), as shown in equation (1):

$$\tau = \sum_{\mathrm{Layer}=1}^{37} (\mathrm{OPSO4} + \mathrm{MOPD} + \mathrm{OPBC} + \mathrm{OPOC} + \mathrm{OPSSa} + \mathrm{OPSSc}) \quad (1)$$

[7] where OPSO4 represents inorganic aerosol optical depth including the sulfate, nitrate, ammonium, and other water-soluble aerosols. MOPD is mineral dust optical depth with the effective radii of dust particles ranging from 0.15 μm to 4.0 μm. OPBC and OPOC are black carbon and organic carbon optical depth, respectively. OPSSa and OPSSc are the optical depth of accumulation and coarse mode sea salt aerosol, respectively. These tracer simulations are all based on the Global Aerosol Data Set (GADS), which consists of aerosol optical properties including wavelength-resolved complex refractive indices and estimates of the aerosol size distributions (geometric mean and standard deviation) at different relative humidities. These properties were then input to a Mie code to generate the additional

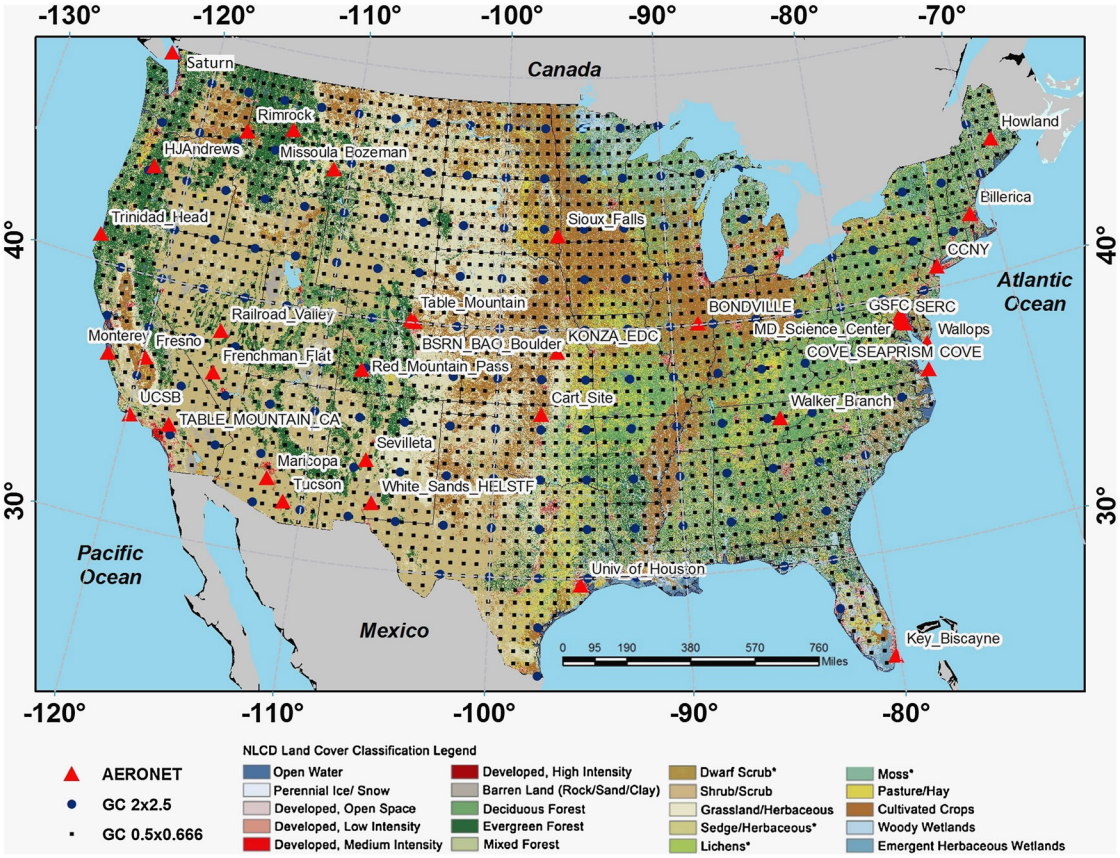

Figure 1. Spatial distribution of GEOS-Chem 2° × 2.5° (blue circles) and 0.5° × 0.666° (nested, black squares) grids in the contiguous United States. Thirty-four AERONET sites containing AOD level 2 data from 2008 to 2010 are shown as red triangles. The NLCD 2006 land cover layer is created by the Multiresolution Land Characteristics consortium (http://www.mrlc.gov/nlcd06_data.php).

parameters, extinction efficiency (Q_{ext}) and effective radius (r_{eff}), necessary for AOD calculations [*Martin et al.*, 2003]:

$$\tau_{tracers} = \frac{3}{4}\frac{Q_{ext}M}{r_{eff}\rho} \quad (2)$$

where M is the column mass loading and ρ is the aerosol density. From equation (2), the two factors that affect GC AOD are the particle mass and the GADS optical properties. The uncertainties in the simulated aerosol mass may be attributed to ground emissions, chemical conversion processes, and meteorological fields (GEOS data). The anthropogenic emissions (SOx, NOx, and CO) in GC version 8.3.2 are based on Emissions Database for Global Atmospheric Research [*Olivier et al.*, 1998]. The sulfate simulation also uses NH3 biofuel and natural source emissions from Global Emissions Inventory Activity [*Benkovitz et al.*, 1996]. The Global Fire Emission Database (GFED) version 2 inventory is used to compute biomass-burning emissions for aerosol species of OC, BC, etc. Biogenic species are emitted following the Model of Emissions of Gases and Aerosols from Nature model inventory [*Guenther et al.*, 2012]. For GADS data, the aerosol optical properties starting with GC version 8.3.1 have been updated to take into account new observations from ground-based aerosol measurements and field campaigns as described in a number of papers [e.g., *Drury et al.*, 2010].

[8] In addition to the global simulations, GC also provides nested grid simulations [*Wang et al.*, 2004] at the native GEOS-5 horizontal resolution of 0.5° × 0.666° for the China/SE Asia region (70°~150° longitude, −11°~52° latitude), North America region (−140°~−70° longitude, 10°~69.5° latitude), and Europe region (−30°~50° longitude, 30°~70° latitude). To produce the nested simulation, the global simulation first needs to run the initial and boundary conditions for all species, then higher-resolution emissions, meteorological data, and the GADS optical properties are used to calculate the AODs within the nested grid. As shown in Figure 1, there are 167 $GC_{2° \times 2.5°}$ grid cells and 1180 $GC_{0.5° \times 0.666°}$ grid cells over the contiguous U.S. Figure 1 also adds the National Land Cover Database (NLCD) 2006 land cover layer for reference, which is partly linked to the ground emission conditions [*Wang et al.*, 2012].

2.2. AERONET Level 2 Aerosol Product

[9] In the contiguous U.S. during the period from 2008 to 2010, there are 34 AERONET sites with Level 2 (quality assured) data (accessed at http://aeronet.gsfc.nasa.gov). Using the longitude lines at 110°W and 90°W, we divided the contiguous U.S. into eastern, western, and central regions. As shown in Figure 1, there are 11 AERONET sites in the Eastern U.S., many of which are located along the eastern seaboard near the Atlantic coast. There are also 9

central and 14 western AERONET sites, many of which contain crops or forest-covered regions as defined in the NLCD 2006 land cover data.

[10] AERONET AOD values are recorded by sun photometers every 15 min in seven spectral bands (nominally 340, 380, 440, 500, 670, 870, and 1020 nm). AERONET AODs at 440 nm and 670 nm were interpolated to 550 nm using the Angström exponent ($\alpha_{440-670}$) in order to compare with GC and satellite data. AERONET observations within 3 h windows around five GC time steps (7 A.M., 10 A.M., 1 P.M., 4 P.M., and 7 P.M. local time converted from UTC time) were averaged and matched to the nearest GC grid cells at 2° × 2.5° and 0.5° × 0.666° resolutions, respectively. Daily, monthly, and annual averages were calculated based on matched data. For $GC_{2^\circ \times 2.5^\circ}$ validation, AERONET values over three East Coast stations (Goddard Space Flight Center, MD_Science_Center, and Smithsonian Environmental Research Center) and two Central stations (Table_Mountain and BSRN_BAO_Boulder) located in one $GC_{2^\circ \times 2.5^\circ}$ grid were combined to compare to the corresponding model simulations.

2.3. MISR Component AOD Data

[11] In addition to AERONET observations, satellite data are often used to evaluate a model's AOD estimations [*Sayer et al*., 2010]. We chose the MISR product since MISR AOD products have been validated against AERONET observations both around the world [*Kahn et al*., 2010] and in the contiguous U.S. [*Liu et al*., 2004a], with a global- and national-retrieved error ($\Delta\tau$) within the larger of ± 0.05 or $\pm 0.2\tau$ and $\pm 0.04 \pm 0.18\tau$, respectively. Furthermore, with the unique multiangle design, MISR-retrieved aerosol microphysical properties contain valuable information of particle size and single-scattering albedo. They can also be used to infer aerosol composition together with atmospheric chemistry model simulations [*Liu et al*., 2009]. The primary deficiency of MISR is the narrow swath of the instrument (~380 km for the nadir-viewing camera) yielding global coverage in 9 days at the equator. Nonetheless, MISR provides a reasonable data source to assess model simulation of different tracers on a global scale.

[12] The MISR Level 2 aerosol data (latest version 22) with a spatial resolution of 17.6 km for the same period and geographic location as the GC simulations were downloaded from the NASA Langley Research Center Atmospheric Sciences Data Center (http://eosweb.larc.nasa.gov). Total column AOD is reported in the MISR product in the parameter "RegBestEstimateSpectralOptDepth," which represents the mean AOD of all mixtures that pass goodness-of-fit tests. However, additional information about aerosol types is also reported in the product, which can be used to determine the fractional contribution of different aerosol components to the total AOD following the approach of [*Liu et al*., 2007a, 2007b]. The green-band (558 nm) AOD for each of the 74 mixtures used in the version 22 retrieval is reported in the parameter "OptDepthPerMixture" and whether or not a particular mixture passed the goodness-of-fit tests is indicated by the field "AerRetrSuccFlagPerMixture." Each mixture is made up of one or more "pure" aerosol components corresponding to inorganic aerosol (components 1, 2, 3, and 6, including sulfate, nitrate, and ammonium), absorbing non-dust species (components 8 and 14, including black carbon, organic carbon, and brown carbon), and dust (components 19 and 21) [*Kahn et al*., 2010]. The total AOD of each component is calculated using equation (3).

$$\tau_{\text{component}-i} = \frac{\sum_{j=1}^{74} \tau_{\text{mixture}-j} \times Fraction_{\text{component}-i \text{ in mixture}-j}}{\text{No. of successful mixtures}} \quad (3)$$

where $\tau_{\text{component}-i}$ is the AOD of component i, $\tau_{\text{mixture}-j}$ is the AOD of mixture j, $\text{Fraction}_{\text{component i in mixture}-j}$ is the contribution of component i to the total AOD for mixture j, and No. of successful mixtures is the number of successful mixtures, which is reported in the MISR product as "NumSuccAerMixture". In this approach, MISR (17.6 km × 17.6 km) cloud-free pixels located in one 0.5° × 0.666° GC grid cell were first averaged (called MISR_{GC} hereinafter). Then the GC simulations at 10 A.M. local time, which roughly corresponds to the MISR overpass time, were sampled for the MISR_{GC} swath. Finally, the 3 years of matched data sets were processed at seasonal time scales for the contiguous U.S. Although *Liu et al*. [2009] showed that this method could successfully simulate the particle concentration such as sulfate aerosol in U.S., two limitations of the current MISR AOD product may also have important impacts on its application. On the one hand, the V22 MISR aerosol climatology lacks certain mixtures such as medium, spherical, absorbing (smoke) particles combined with dust [*Kahn et al*., 2010]. On the other hand, if many different mixtures successfully pass the retrieval criteria [*Liu et al*., 2007a], equation (3) might reflect more on aerosol climatology than specific aerosol properties.

3. Results and Discussion

3.1. Validation of GC Column AOD With AERONET Observations

[13] Overall, the numbers of daily mean records from 2008 to 2010 for the 34 AERONET sites over the contiguous U.S. are 11,041 for $GC_{2^\circ \times 2.5^\circ}$ (Figure 2a) and 11,906 for GC-nested simulations (Figure 2b), respectively. The number of matched samples between model and ground truth is larger than that in any satellite-only validation study over a similar time period because the CTM can simulate aerosols in all conditions without the limitations of cloud contamination, bright underlying surfaces, or the temporal and spatial constraints of an orbital swath. Linear regression of the $GC_{2^\circ \times 2.5^\circ}$ AOD against the AERONET observations yields an r of 0.6, a slope of 0.51, and an intercept of 0.03, which indicates that the $GC_{2^\circ \times 2.5^\circ}$ underpredicts AOD values relative to AERONET in most conditions. In addition to the impact of a potentially inaccurate emissions inventory and GADS optical properties that may not adequately represent the true aerosols, the coarse spatial resolution of $GC_{2^\circ \times 2.5^\circ}$ simulations may also introduce other uncertainties. For example, when the three East Coast sites are combined, the correlation between AERONET and $GC_{2^\circ \times 2.5^\circ}$ (slope:0.52, r:0.64) is better than the comparison for individual sites (slope:0.48, r:0.59). *Jiang et al*. [2007] found that in comparisons between MISR and AERONET in Beijing, some biases could be attributed to aerosol spatial variability, especially for heavily polluted environments. It is likely that similar biases exist in the comparison between $GC_{2^\circ \times 2.5^\circ}$ and

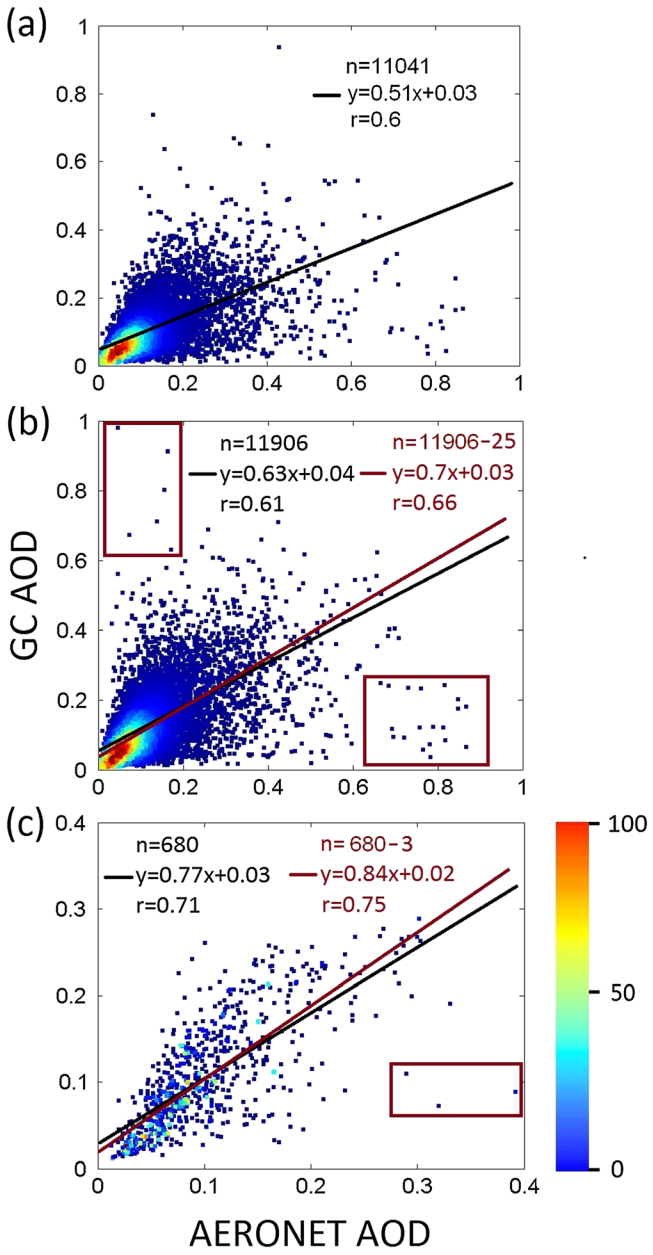

Figure 2. Validation of GC AOD at a horizontal resolution of (a) 2° × 2.5°daily mean, (b) 0.5° × 0.666° daily mean, and (c) 0.5° × 0.666° monthly mean using AERONET observations. The linear regression line for all data set is shown as the black line. The linear regression line without few outliers (inside the red box) is shown as the red line. Color bar represents the number of data with those particular ordered pair values.

AERONET performed here. Compared to the $GC_{2^\circ \times 2.5^\circ}$ simulations, the GC simulations run with a horizontal resolution of 0.5° × 0.666° are more comparable to the standard size of validation domains for satellites, such as a 50 km × 50 km box (5 × 5) for MODIS [*Chu et al.*, 2002] and 52.8 km × 52.8 km (3 × 3) box for MISR [*Kahn et al.*, 2010]. As shown in Figure 2b, the slope improves from 0.51 to 0.63 when using the nested data, which is better able to capture high values of aerosol loading for species with short lifetimes [*Yu et al.*, 2012a]. In addition, AERONET observation is for clear-sky conditions, while at GC grid box, it can be partially cloudy. The higher-resolution nested data are likely to reduce sampling bias such as cloud contamination and other bias. Many of the points where GC underestimates the AOD relative to AERONET (Figure 2b, lower right corner) are from coastal sites (i.e., over southern California and around the Chesapeake Bay) in the summer. Points where GC overestimates the AOD relative to AERONET (Figure 2b, upper left corner) all occur for inland sites in the northwestern portion of the U.S. (i.e., Rimrock, Missoula, and Bozeman). This might indicate that the aerosol conditions in this region are not well characterized by the current emission data, meteorological fields, or GADS optical data. The errors related to different GC components will be further analyzed in the following sections. The regression after removing 25 outliers (inside the boxes in Figure 2b), which make up ~0.2% of the total

Table 1. Statistics for AERONET and GC AOD Variables by Season, Hour, and Geographical Regions

	Variables	*N*1	*N*2	Mean	Min	Max	Diff	Slope	Intercept	*r*
Spring	AERONET	34	3410	0.114	0.02	0.407	0.042	0.808	0.037	0.693
	GC			0.13	0.023	0.481				
Summer	AERONET	33	3456	0.152	0.026	0.814	0.063	0.465	0.067	0.493
	GC			0.14	0.02	0.625				
Fall	AERONET	33	2580	0.088	0.012	0.498	0.045	0.717	0.03	0.614
	GC			0.093	0.008	0.536				
Winter	AERONET	34	2460	0.06	0.009	0.283	0.031	0.682	0.028	0.544
	GC			0.069	0.007	0.326				
7 A.M.	AERONET	34	7604	0.107	0.011	0.57	0.049	0.612	0.048	0.594
	GC			0.114	0.009	0.533				
10 A.M.	AERONET	34	9432	0.102	0.01	0.607	0.048	0.641	0.038	0.579
	GC			0.106	0.008	0.532				
1 P.M.	AERONET	34	9411	0.103	0.011	0.605	0.045	0.592	0.036	0.589
	GC			0.104	0.008	0.533				
4 P.M.	AERONET	34	9108	0.109	0.012	0.649	0.05	0.627	0.040	0.592
	GC			0.113	0.009	0.61				
7 P.M.	AERONET	30	2065	0.132	0.022	0.63	0.057	0.493	0.063	0.476
	GC			0.129	0.022	0.628				
East	AERONET	11	3829	0.146	0.024	0.641	0.067	0.635	0.077	0.626
	GC			0.17	0.018	0.56				
Central	AERONET	9	3350	0.094	0.011	0.441	0.037	0.705	0.03	0.668
	GC			0.093	0.007	0.414				
West	AERONET	14	4727	0.088	0.011	0.603	0.041	0.414	0.041	0.329
	GC			0.078	0.009	0.513				

*N*1 is the number of AERONET stations used; *N*2 refers to sample days.
Min and Max are calculated by averaging the top 1% min and max value to reduce the outliers, rather than just selecting one value.
Diff is calculated as the mean of absolute value of daily GC-AERONET.
Spring is March through May, summer is June through August, fall is September through November, and winter is December through February.
The GC local time for AERONET represents 3 h. 7 A.M. is 6: 00 A.M. to 9:00 A.M., 10 A.M. is 9: 00 A.M. to 12:00 P.M., 1 P.M. is 12: 00 P.M. to 3:00 P.M., 4 P.M. is 3: 00 P.M. to 6:00 P.M., and 7 P.M. is 6: 00 P.M. to 9:00 P.M.

11,906 samples, has an *r* of 0.66 and a slope of 0.7. To test the ability of the GC model for simulating AOD in a longer time-averaging window, Figure 2c shows the comparison between $GC_{0.5^\circ \times 0.667^\circ}$ and AERONET monthly mean AOD (note the change in scale from previous two plots). As expected, monthly averaging appears to significantly smooth the model's instantaneous noise. Three outliers are found in western and central sites in the summer, because of many low values for the whole month. After elimination of these outliers, the correlation and regression both improve further, yielding an *r* of 0.75 and a slope of 0.84.

[14] Summary statistics for $GC_{0.5^\circ \times 0.667^\circ}$ and AERONET values for the entire data set, as well as stratified by season, hour, and by location, are presented in Table 1. Seasonal comparison shows that AERONET has a slightly wider range (0.009–0.814) in AOD values, particularly for high AOD, when compared to GC estimates (0.007–0.625). AOD values varied greatly by season for both GC and AERONET; AODs in the summer (AERONET: 0.152, GC: 0.14) were more than twice as high as in the winter (AERONET: 0.06, GC: 0.069). Overall, GC AOD mean values are comparable with AERONET observations, with a slight overestimation in the summer and underestimation during other seasons. However, the mean daily difference between AERONET and GC was significant in all four seasons, almost amounting to 50% of the AERONET seasonal mean. The slope, intercept, and correlation coefficient were better in the spring (slope:0.808, intercept:0.037, *r*:0.693) and the fall (slope:0.717, intercept:0.03, *r*:0.614) versus the summer (slope:0.465, intercept:0.067, *r*:0.493) or the winter (slope:0.682, intercept:0.028, *r*:0.544). When considering hourly variations, the daytime (7 A.M. to 4 A.M.) aerosol observations from GC and AERONET have a similar value range and linear relationship. Although both AERONET and $GC_{0.5^\circ \times 0.667^\circ}$ show the aerosol pollutants reaching their peak at 7 P.M. (6 P.M. ~ 8 P.M.), with a mean AOD of ~0.13, there is a large discrepancy and weak correlation (slope: 0.493, *r*: 0.476). There are several contributing factors. First, 68% AERONET measurements around 7 P.M. are found during summer, in which GC usually shows poor performance. Second, near-source aerosol concentrations around peak AOD may also play an important role at nighttime. Finally, point AERONET measurements do not represent a large GC grid cell well at 7 P.M. because nighttime atmospheric stability limits aerosol mixing. This is supported by our observation that the correlation between $GC_{2^\circ \times 2.5^\circ}$ and AERONET is worse (slope: 0.34, *r*: 0.44). Geographically, eastern sites generally had higher and more variable AOD values than central and western sites. Linear regression analysis shows that the slope between daily AERONET and GC AODs was the highest over central sites (0.705) and lowest over western sites (0.414), which means that GC underestimates AODs especially on heavy air pollution days in these western regions. Table 1 also indicates that the correlation coefficients in the eastern (0.626) and central (0.668) sites were better than those in western sites (0.329). Additional correlation analysis related to seasonal differences by region is presented in Table 2. Over the Eastern and Central U.S., GC performs well during spring, fall, and winter seasons but underestimates the AOD values in the summer by a factor of ~2. Our results are consistent with the study of *Veefkind et al.* [2011], who found that such discrepancies are most likely due to too strong precipitation and too low secondary organic aerosols formation in the model. Over the Western U.S., GC in the spring shows a

Table 2. Statistics for the Seasonal Correlations Between AERONET and GC AOD by Region

	East			Central			West		
	Slope	Intercept	r	Slope	Intercept	r	Slope	Intercept	r
Spring	0.757	0.078	0.656	0.739	0.034	0.681	0.534	0.045	0.624
Summer	0.481	0.101	0.547	0.386	0.075	0.312	0.197	0.074	0.205
Fall	1.198	0.031	0.668	1.05	−0.005	0.756	0.241	0.029	0.387
Winter	0.874	0.047	0.617	1.016	−0.001	0.755	0.163	0.036	0.284

relatively comparable agreement against AERONET but has much smaller slopes and correlation coefficients for the other seasons.

3.2. Comparison of GC Component AOD With MISR Retrievals

[15] Figure 3 shows the ground-observed, model-simulated (left column), and satellite-retrieved (right column) AOD distributions. The results presented in Figure 3 indicate that on average, both the model and satellite results yield the highest AOD in summer (GC: 0.124, MISR: 0.164), followed by spring (GC: 0.121, MISR: 0.16), fall (GC: 0.109, MISR: 0.106), and winter (GC: 0.077, MISR: 0.098). Geographically, there are large differences. Model simulations are mainly controlled by emission, transport, and hygroscopic properties of aerosols; high values of AOD are persistently located over relatively populated and polluted regions such as the Eastern U.S. GC AOD in eastern regions is a factor of 2 ~ 3 times higher than the AOD in the western region. An obvious line can be found around longitude 100°W at the foothills of the Rocky Mountains (Figure 3, left column), which the model maybe made more of a barrier than they actually are. Compared to the ground-based AOD distribution (Figure 3, right column), GC was unable to capture the AERONET aerosol variability, especially for western-polluted regions such as Fresno.

[16] The uncertainties in satellite AOD are usually attributed to surface reflectance estimation, the composition of the assumed aerosols, cloud screening, and so on [*Chu et al*., 2002]. For example, errors of 0.01 in assumed surface reflectance may lead to errors on the order of 0.1 for MODIS AOD retrieval [*Kaufman et al*., 1997]. Unlike traditional sensors such as MODIS, MISR's nine cameras greatly reduced the impact of surface reflectance uncertainties [*Diner et al*., 2005]. Even so, Figure 3 indicates that there is an agreement between MISR retrievals and NLCD land cover, which may be due to added noise of bright targets over Western U.S. As shown in Figure 3 (right column), the highest values of AOD (~1) are persistently located over the Great Salt Lake Desert areas covered by white sand, as reported in the study of *van Donkelaar et al*. [2010]. Nevertheless, other studies have shown that MISR retrieves reliable AODs in dusty regions [*Martonchik et al*., 2004].

[17] We also examined the MISR product using AERONET data following standard validation methods [*Liu et al*., 2004a]. Our results are very similar to the previous studies [*Chatterjee et al*., 2010]. Overall, for the contiguous U.S. during the period from 2008 to 2010, MISR retrievals have a strong correlation to AERONET data ($y = 0.82x + 0.05$, $r = 0.7$). Even in Western U.S., the agreement ($y = 0.89x + 0.06$, $r = 0.63$) is much better than for the GC simulations, which implies that MISR is better able to capture aerosol variability than GC over these regions. However, the MISR AOD retrievals show biases when AOD is very high (greater than ~0.4) [*Kahn et al*., 2010] or very low [*Liu et al*., 2004a]. For eastern regions, MISR produces a slight underestimation ($y = 0.81x + 0.03$, $r = 0.84$), especially for higher AODs along the East Coast in the summer (Figure 3d). *Liu et al*. [2004a] also indicated that in low optical depth situations, MISR AOD retrievals may be biased high. In this analysis, we limited our data to those with column AOD value greater than or equal to 0.05, which reduced the raw data by about 17% (43401/253938 MISR_{GC} pixels). There was a little change in the AOD distribution in the spring and summer, but the AOD value in the winter and fall when low values are common increased by 23% and 24%, respectively. Therefore, quantitative intercomparison of the model simulations, the satellite retrievals, and the ground truth should be done with caution because the large discrepancies could be due to (1) model uncertainties such as the emission inventory and GADS data; (2) satellite retrieval errors caused by cloud screening, surface reflectance uncertainties, and assumptions in the aerosol model climatology; and (3) sampling difference in both space and time with ground-based data. Nevertheless, such intercomparisons still provide useful information on the strengths and weaknesses of both approaches, and coupling model simulations with the satellite retrievals as was done by *Drury et al*. [2008] and *Wang et al*. [2010] has demonstrated improved AOD agreement with AERONET.

[18] To investigate the relative importance of each aerosol type, we also calculated the MISR component AOD using equation (3) to compare with the GC tracers. Figures 4–6 are similar to Figure 3 but represent the seasonal distribution of optical depth of inorganic aerosol, dust, and absorbing non-dust particles, respectively. In Figure 4, both GC and MISR show a large contribution of inorganic aerosol to total AOD, with a national annual mean of 0.071 for GC and 0.089 for MISR. Moreover, the spatial and temporal distribution is similar to Figure 3, which indicates that inorganic aerosol is the most prevalent pollutant in the U.S. High inorganic aerosol polluted areas found in the GC model were concentrated in the Eastern and Central U.S., including Indiana, Illinois, Kentucky, Ohio, Arkansas, and Pennsylvania. These states were reported to emit the highest levels of air pollution in terms of pounds of power plant emissions, based on statistics kept by the Environmental Integrity Project (http://www.environmentalintegrity.org/). Similar to GC, MISR also shows heavy inorganic aerosol distribution in these states, but with relatively lower AOD in summer, fall, and winter. On the other hand, MISR's retrieved inorganic AOD over most western regions is higher than GC in all four seasons. One possible reason could be MISR's ability to distinguish different aerosol mixtures from one another. Following the method of *Liu et al*. [2007a], we produced statistics using 3 years of

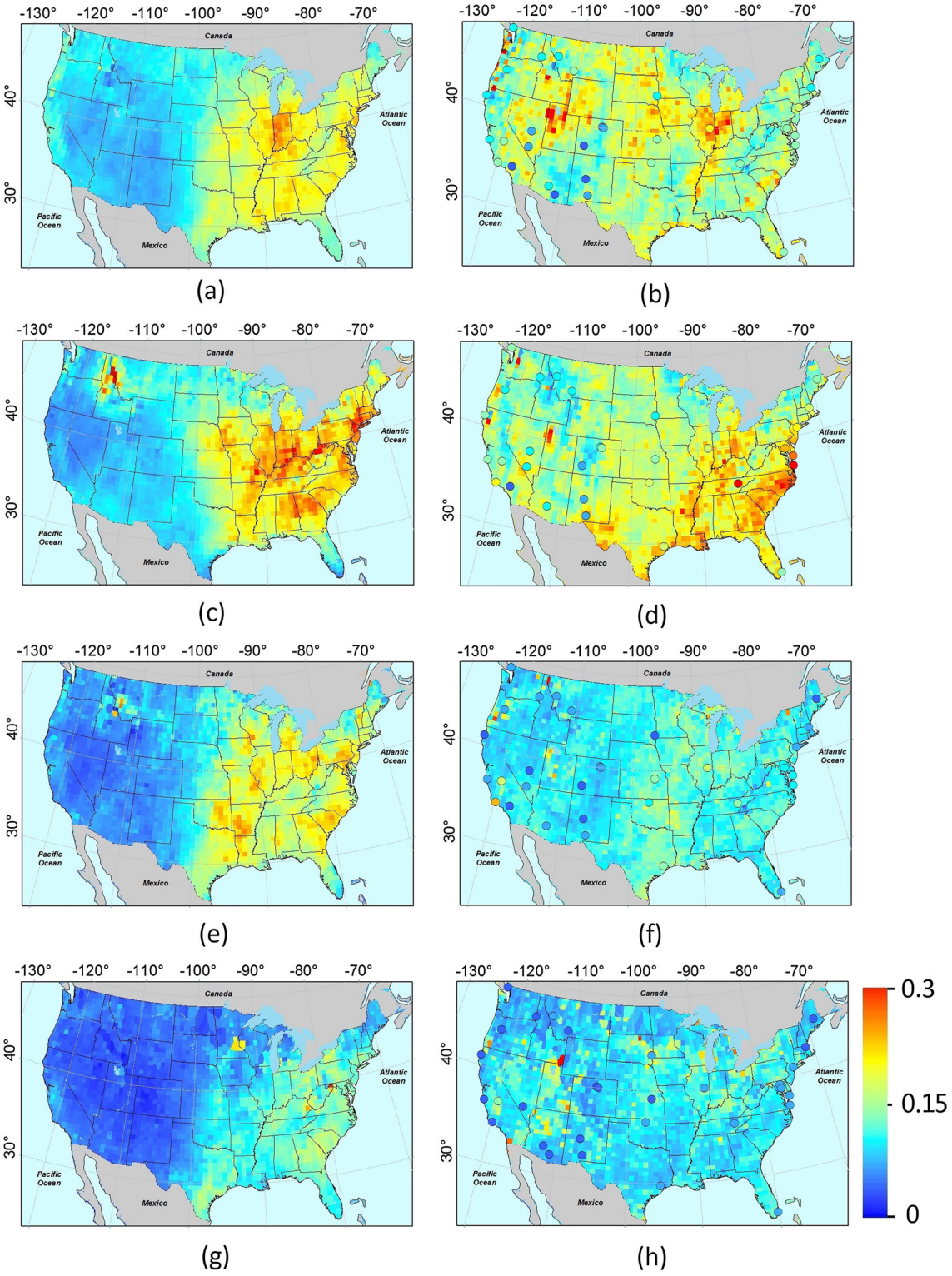

Figure 3. Distributions of seasonal average AOD at 550 nm from 2008 to 2010 in (a, b) spring, (c, d) summer, (e, f) fall, and (g, h) winter. (left column) GC simulations are temporally and spatially matched with (right column) MISR cloud-free conditions. AERONET AOD distributions are superposed on the MISR maps.

MISR data over 34 AERONET sites. Although the version 22 product is able to distinguish non-dust particles from dust particles with an error of approximately 4%, there is still 15% uncertainty for distinguishing the non-light-absorbing (inorganic) and light-absorbing (absorbing non-dust) aerosols, consistent with previous sensitivity studies [*Liu et al.*, 2007a]. Nevertheless, high inorganic AOD values seen in California and southern Texas in the MISR data better match populated

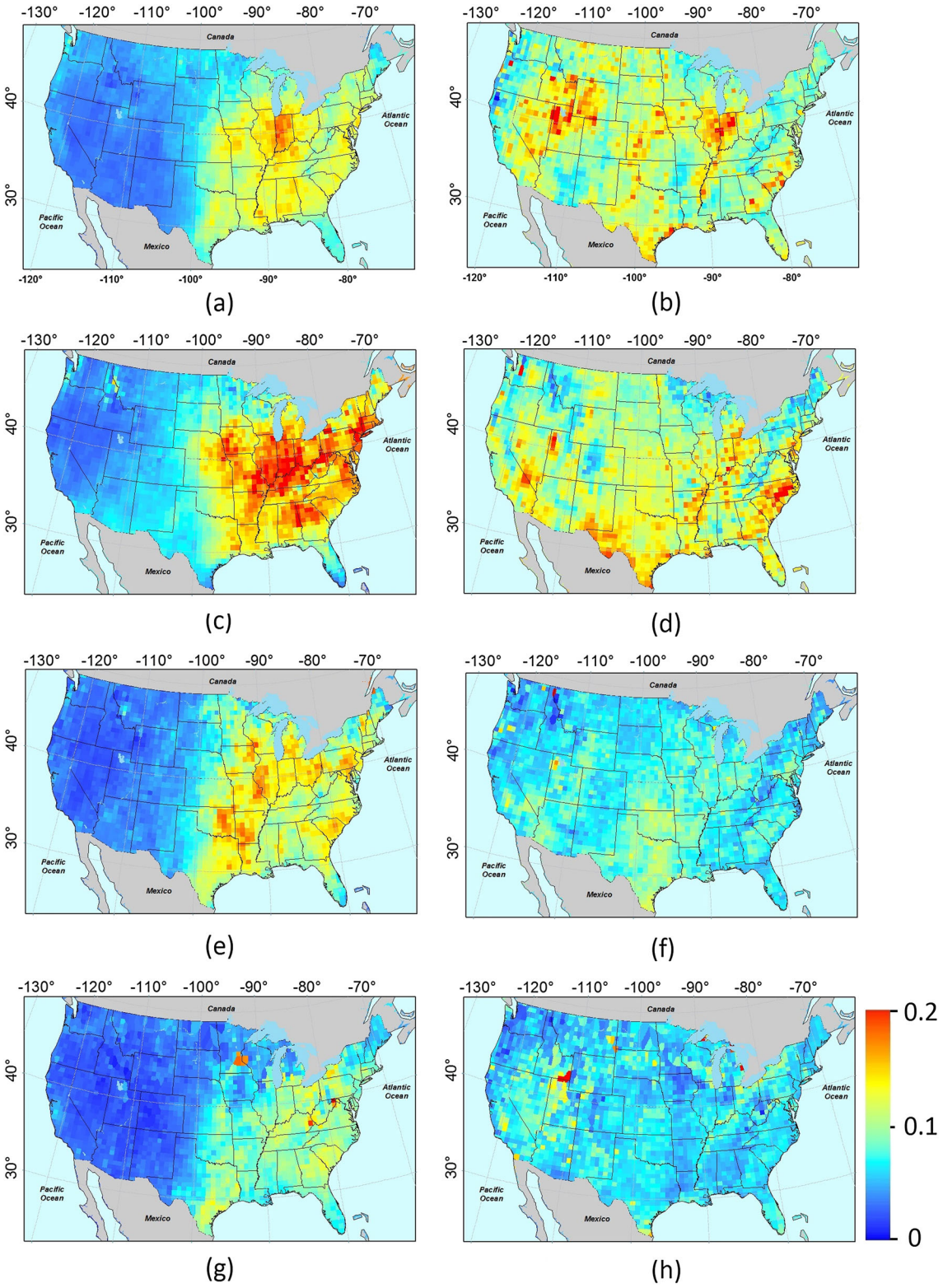

Figure 4. Same as Figure 3 but for inorganic AOD distribution, note that the color bar is from 0 to 0.2.

regions with heavy fossil fuel usage. GC was unable to capture the inorganic aerosol pollution over the Western U.S. It may be caused by the rapid aerosol sink in the GC model due to too strong precipitation [*Veefkind et al.*, 2011].When assessing the GC-AERONET validation (section 3.1), the above findings indicate that the substantial underestimation seen in the GC inorganic AOD distribution may be explained to a large extent by the low bias (Figure 2b) introduced in the Western U.S., especially for heavily polluted summer days.

[19] For GC dust, annual average simulated AOD is 0.013, with the largest national mean value of 0.033 in spring, and other seasons are averaging below 0.01. This finding can be

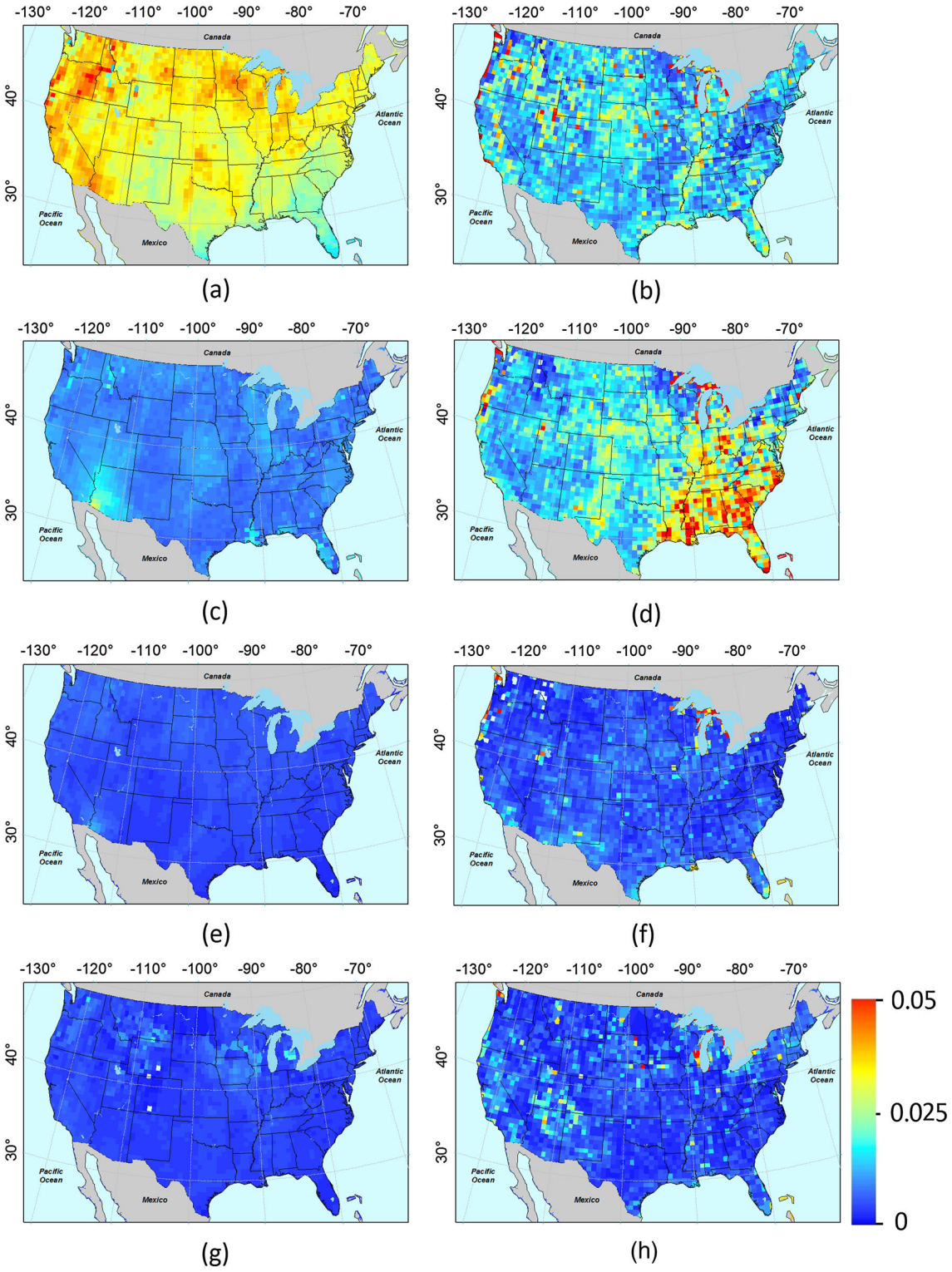

Figure 5. Same as Figure 3 but for mineral dust AOD distribution, note that the color bar is from 0 to 0.05.

attributed to the transport of Asian fine dust into North America during spring. *Yu et al*. [2012b] found that approximately 140 Tg of dust was exported from East Asia in 2005. After the trans-Pacific transport, 56 Tg of dust reached the West Coast of North America, although there are large uncertainties on these estimates. The contribution of fine Asian dust becomes weaker in the summer and fall and decreases to 30–50% of the springtime maximum over the Eastern U.S. [*Fairlie et al*., 2007]. However, mean dust AOD (0.019) from MISR in the spring is significantly lower than GC. This discrepancy is mainly caused by GC overestimation on mineral dust concentrations during the trans-Pacific dust events, which is much higher than the data observed in the Transport and Chemical Evolution over the

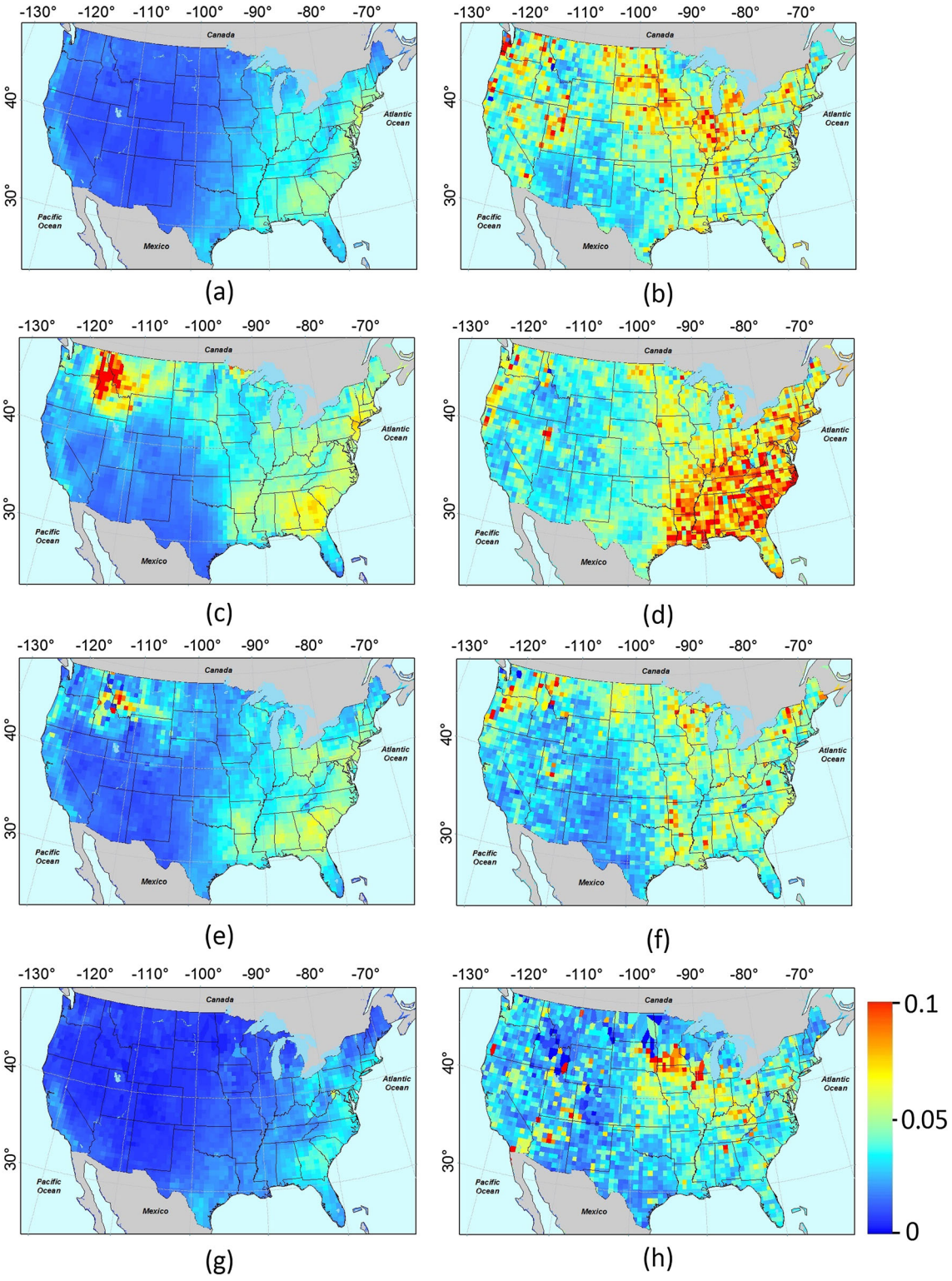

Figure 6. Same as Figure 3 but for absorbing non-dust species AOD distribution, note that the color bar is from 0 to 0.1.

Pacific and Asian Pacific Regional Aerosol Characterization Experiment aircraft campaigns of spring 2001 [*Fairlie et al.*, 2007]. In addition to the imperfect GC dust sources characterization, it lacks MISR's capability for characterizing nonspherical particles. For regions downwind of dust sources (such as over Southwestern U.S. in the dusty season), the phase functions of spherical and nonspherical particles are both important for the accurate AOD calculation [*Wang et al.*, 2012]. For MISR, lack of very absorbent, plate-like dust particles in the retrieval algorithm may lead to the underestimation of MISR dust AOD [*Kalashnikova et al.*, 2005]. In the summer, the largest difference is found over

the Southeastern U.S. where MISR dust AOD is approximately a factor of 3 to 4 higher than GC simulations. This could be due to the import of Sahara dust, which travels farther south (towards the Amazon) during the spring season and farther north (towards the Caribbean and southern US) during the summer [*Ridley et al*., 2012]. Our results are consistent with those found by *Generoso et al*. [2008], who reported that GC-derived attenuated backscatter profiles over the Atlantic were weak compared to the CALIPSO lidar observations, particularly during the summertime. Both findings suggest that dust deposition during plume transport may be too strong in the GC model. Overall, the annual average MISR dust AOD (0.014) is almost equal to GC, accounting for less than 10% of the total AOD, which is lower than the ~25% seen in previous studies [*Liu et al*., 2004b].

[20] GC-absorbing non-dust aerosol usually appears over the Northwest and East Coast of U.S., which is mainly covered by evergreen, deciduous, and mixed forest. Figure 6 shows that the GC-absorbing non-dust AOD in the West reaches the largest values in summer and the lowest values in winter. This spatial-temporal pattern is consistent with the smoke emission, in which *Ichoku et al*. [2008] showed that the peak months are from May to October for the Western U.S. However, it is clear that GC overestimates AOD (~1) in several states in the Northwest U.S. (i.e., Idaho and Montana) during summer. Referring back to Figure 2b, it appears that this overestimation also contributed to the high outliers in the AERONET comparison (Figure 2b, top left corner). A possible reason for this result is the GC version 8.3.2 model, which uses the GFED version 2 8 day emissions for the years 2001–2007 (accessed at http://www.globalfiredata.org/) to reproduce the simulations for years 2008–2010. The old fire emission data predicts larger amounts of burned areas, which results in model estimates of higher-absorbing non-dust AOD. For example, the Murphy Complex Fire in 2007 was the third largest wildfire in the United States in the past 15 years (accessed at the report of National Interagency Fire Center at http://www.nifc.gov/), causing the 2007 fire emissions inventory in this region to be significantly higher than later years. This problem could potentially be solved by using the latest GFED Version 3 monthly biomass inventory [*van der Werf et al*., 2010]. Given a quantitative relationship between AOD and biomass-burning emissions in each geographic region [*Petrenko et al*., 2012], we also suggest that GC could couple high-quality satellite AOD such as that from MISR to constrain the biomass-burning source strength. In the East, GC-absorbing non-dust AOD shows little seasonal change except in the summer, most likely because of the dominance of the anthropogenic emissions from diesel and coal combustion, and there is no distinct peak month in the biomass-burning emissions from prescribed fires [*Liu*, 2004]. The relatively high values in the summer may be because the anthropogenic and fire effluences from Western North America are mostly transported north and east, eventually merging with Eastern U.S. pollution outflow to the Atlantic [*Li et al*., 2005]. However, the GC-absorbing non-dust AOD is still significantly underestimated compared to MISR in most central and eastern regions in all seasons and resulted in the annual mean values (0.025) that are much lower than MISR (0.041). There are several possible reasons for this discrepancy. First, the aerosol model used in the MISR component AOD calculation may be inappropriate. We used components 8 and 14 for absorbing non-dust species, which also includes some inorganic and sea salt fine particles, according the definition of these MISR components [*Kahn et al*., 2010]. As mentioned before, this assumption is likely to cause higher-absorbing non-dust and lower inorganic aerosol levels (Figure 4, right column). Second, as opposed to the large wildfires in the western U.S., the smaller prescribed fires are often underrepresented in the emission inventories [*Wang et al*., 2007]. Third, because the black carbon simulation is sensitive to the smoke injection height but the GC model does not use constraints on the injection height, this will decrease the black carbon column in Eastern U.S. by 10% to 20% [*Chen et al*., 2009]. Finally, the presence of elevated aerosol layers from long-range transport, such as the biomass-burning outflow across the Gulf of Mexico [*Wang et al*., 2009], may be detected by MISR but not represented in the model.

4. Conclusions

[21] In this study, the GC AOD of total column and main tracers over the contiguous U.S. from 2008 to 2010 were compared using data from 34 AERONET sites and MISR satellite retrievals. Data are compared using 3 h temporal averages for AERONET, nearest GC-AERONET points, and 0.5° × 0.667° surrounding averaged retrievals for MISR. A linear regression analysis, using $GC_{2^\circ \times 2.5^\circ}$ AOD as the response, yielded a slope of 0.51 and intercept of 0.03, suggesting that $GC_{2^\circ \times 2.5^\circ}$ may underestimate AERONET AOD, especially at high values. After applying a $GC_{0.5^\circ \times 0.667^\circ}$ nested model to control the spatial variability, eliminating several outliers, and averaging instantaneous values in a sustained duration to smooth noise, we achieved the result with a slope of 0.84 and an r of 0.75. Together, the above findings indicate the agreement between the model and ground-based measurements could be improved using higher spatial and longer temporal resolution data. Summary statistics for $GC_{0.5^\circ \times 0.667^\circ}$ and AERONET values stratified temporally and geographically show that (1) overall, the data range (min, max) and mean values of the entire $GC_{0.5^\circ \times 0.667^\circ}$ are strongly correlated with AERONET AOD; (2) on seasonal average, summer AODs are more than twice as high as in the winter, with both seasons having worse agreement (lower r and slope) than spring and fall against AERONET; (3) for hourly data, the air mass loading peaked in the evening but with weak correlation due to stable atmosphere; and (4) geographically, eastern and central regions have higher AOD values and better regressions than the western sites.

[22] Using the method of *Liu et al*. [2009], we further calculated the optical depth of individual aerosol types from MISR to perform large-scale comparisons. Both GC and MISR results show that the contiguous U.S. is dominated by inorganic aerosol, followed by absorbing non-dust species, then dust. However, there are large geographical and seasonal differences among these aerosol types. GC significantly underestimates inorganic aerosol levels throughout the year in the Western U.S., as well as dust levels during summer in the Eastern U.S., but overestimates summer-absorbing non-dust species over the northwest compared to the MISR retrievals. These discrepancies may be caused

by (1) the GC uncertainties associated with the simulation of aerosol mass, such as local inorganic aerosol emissions, fire events, and dust transport; (2) MISR retrieval errors due to the bright surface reflectance over Western U.S. and inappropriate optical properties used for the absorbing non-dust aerosol; and (3) the impact of GADS aerosol optical properties (hygroscopic factors, complex refractive indices, and size distributions) and meteorological fields (GEOS data), which are not analyzed in this approach. Though large uncertainties exist in the quantitative comparison between satellite-driven and model-simulated AOD, this study provides useful information on the strengths and weaknesses of both.

[23] **Acknowledgments.** This work was supported by the National Natural Science Foundation of China for Young Scholar (grant 41101400) and the Key Program (grant 41130528) and the Strategic Priority Research Program of the Chinese Academy of Sciences (grant XDB05020100). We thank the principal investigators (PI) and their staff for establishing and maintaining the AERONET sites used in this investigation. The work of Shenshen Li and Yang Liu is partially supported by the MISR science team at the Jet Propulsion Laboratory led by David Diner (subcontract 1363692) and by NASA Applied Science Program managed by John Haynes (agency grant NNX09AT52G and NNX11AI53G, grant PI: Y. Liu). Portions of this work were carried out at the Jet Propulsion Laboratory, California Institute of Technology, under a contract with NASA. We acknowledge the technical support of Zhongting Wang and Meng Fan.

References

Benkovitz, C. M., M. T. Scholtz, J. Pacyna, L. Tarrason, J. Dignon, E. C. Voldner, P. A. Spiro, J. A. Logan, and T. E. Graedel (1996), Global gridded inventories of anthropogenic emissions of sulfur and nitrogen, *J. Geophys. Res.*, *101*(D22), 29,239–29,253.

Bey, I., D. J. Jacob, R. M. Yantosca, J. A. Logan, B. D. Field, A. M. Fiore, Q. B. Li, H. G. Y. Liu, L. J. Mickley, and M. G. Schultz (2001), Global modeling of tropospheric chemistry with assimilated meteorology: Model description and evaluation, *J. Geophys. Res.*, *106*(D19), 23,073–23,095.

Chatterjee, A., A. M. Michalak, R. A. Kahn, S. R. Paradise, A. J. Braverman, and C. E. Miller (2010), A geostatistical data fusion technique for merging remote sensing and ground-based observations of aerosol optical thickness, *J. Geophys. Res.*, *115*, D20207, doi:10.1029/2009JD013765.

Chen, Y., Q. Li, J. T. Randerson, E. A. Lyons, R. A. Kahn, D. L. Nelson, and D. J. Diner (2009), The sensitivity of CO and aerosol transport to the temporal and vertical distribution of North American boreal fire emissions, *Atmos. Chem. Phys.*, *9*(17), 6559–6580.

Chin, M., P. Ginoux, S. Kinne, O. Torres, B. N. Holben, B. N. Duncan, R. V. Martin, J. A. Logan, A. Higurashi, and T. Nakajima (2002), Tropospheric aerosol optical thickness from the GOCART model and comparisons with satellite and Sun photometer measurements, *J. Atmos. Sci.*, *59*(3), 461–483.

Chu, D. A., Y. J. Kaufman, C. Ichoku, L. A. Remer, D. Tanre, and B. N. Holben (2002), Validation of MODIS aerosol optical depth retrieval over land, *Geophys. Res. Lett.*, *29*(12), 8007, doi:10.1029/2001GL013205.

Diner, D. J., J. V. Martonchik, R. A. Kahn, B. Pinty, N. Gobron, D. L. Nelson, and B. N. Holben (2005), Using angular and spectral shape similarity constraints to improve MISR aerosol and surface retrievals over land, *Remote Sens. Environ.*, *94*(2), 155–171.

Drury, E., D. J. Jacob, J. Wang, R. J. D. Spurr, and K. Chance (2008), Improved algorithm for MODIS satellite retrievals of aerosol optical depths over western North America, *J. Geophys. Res.*, *113*, D16204, doi:10.1029/2007JD009573.

Drury, E., D. J. Jacob, R. J. D. Spurr, J. Wang, Y. Shinozuka, B. E. Anderson, A. D. Clarke, J. Dibb, C. McNaughton, and R. Weber (2010), Synthesis of satellite (MODIS), aircraft (ICARTT), and surface (IMPROVE, EPA-AQS, AERONET) aerosol observations over eastern North America to improve MODIS aerosol retrievals and constrain surface aerosol concentrations and sources, *J. Geophys. Res.*, *115*, D14204, doi:10.1029/2009JD012629.

Fairlie, T. D., D. J. Jacob, and R. J. Park (2007), The impact of transpacific transport of mineral dust in the United States, *Atmos. Environ.*, *41*(6), 1251–1266.

Generoso, S., I. Bey, M. Labonne, and F. M. Breon (2008), Aerosol vertical distribution in dust outflow over the Atlantic: Comparisons between GEOS-Chem and Cloud-Aerosol Lidar and Infrared Pathfinder Satellite Observation (CALIPSO), *J. Geophys. Res.*, *113*, D24209, doi:10.1029/2008JD010154.

Guenther, A. B., X. Jiang, C. L. Heald, T. Sakulyanontvittaya, T. Duhl, L. K. Emmons, and X. Wang (2012), The Model of Emissions of Gases and Aerosols from Nature version 2.1 (MEGAN2.1): An extended and updated framework for modeling biogenic emissions, *Geosci. Model Dev.*, *5*(6), 1471–1492.

Holben, B. N., et al. (1998), AERONET—A federated instrument network and data archive for aerosol characterization, *Remote Sens. Environ.*, *66*(1), 1–16.

Ichoku, C., L. Giglio, M. J. Wooster, and L. A. Remer (2008), Global characterization of biomass-burning patterns using satellite measurements of fire radiative energy, *Remote Sens. Environ.*, *112*(6), 2950–2962.

Jaegle, L., P. K. Quinn, T. S. Bates, B. Alexander, and J. T. Lin (2011), Global distribution of sea salt aerosols: New constraints from in situ and remote sensing observations, *Atmos. Chem. Phys.*, *11*(7), 3137–3157.

Jiang, X., Y. Liu, B. Yu, and M. Jiang (2007), Comparison of MISR aerosol optical thickness with AERONET measurements in Beijing metropolitan area, *Remote Sens. Environ.*, *107*(1–2), 45–53.

Johnson, M. S., N. Meskhidze, and V. P. Kiliyanpilakkil (2012), A global comparison of GEOS-Chem-predicted and remotely-sensed mineral dust aerosol optical depth and extinction profiles, *J. Adv. Model. Earth Syst.*, *4*, M07001, doi:10.1029/2011MS000109.

Kahn, R. A., B. J. Gaitley, M. J. Garay, D. J. Diner, T. F. Eck, A. Smirnov, and B. N. Holben (2010), Multiangle Imaging SpectroRadiometer global aerosol product assessment by comparison with the Aerosol Robotic Network, *J. Geophys. Res.*, *115*, D23209, doi:10.1029/2010JD014601.

Kalashnikova, O. V., R. Kahn, I. N. Sokolik, and W. H. Li (2005), Ability of multiangle remote sensing observations to identify and distinguish mineral dust types: Optical models and retrievals of optically thick plumes, *J. Geophys. Res.*, *110*, D18S14, doi:10.1029/2004JD004550.

Kaufman, Y. J., D. Tanre, L. A. Remer, E. F. Vermote, A. Chu, and B. N. Holben (1997), Operational remote sensing of tropospheric aerosol over land from EOS moderate resolution imaging spectroradiometer, *J. Geophys. Res.*, *102*(D14), 17,051–17,067.

Li, Q. B., D. J. Jacob, R. Park, Y. X. Wang, C. L. Heald, R. Hudman, R. M. Yantosca, R. V. Martin, and M. Evans (2005), North American pollution outflow and the trapping of convectively lifted pollution by upper-level anticyclone, *J. Geophys. Res.*, *110*, D10301, doi:10.1029/2004JD005039.

Lim, S. S., et al. (2012), A comparative risk assessment of burden of disease and injury attributable to 67 risk factors and risk factor clusters in 21 regions, 1990–2010: A systematic analysis for the Global Burden of Disease Study 2010, *Lancet*, *380*(9859), 2224–2260, doi:10.1016/S0140-6736(12)61766-8.

Lin, J. T., Z. Liu, Q. Zhang, H. Liu, J. Mao, and G. Zhuang (2012), Modeling uncertainties for tropospheric nitrogen dioxide columns affecting satellite-based inverse modeling of nitrogen oxides emissions, *Atmos. Chem. Phys.*, *12*(24), 12,255–12,275.

Liu, Y. Q. (2004), Variability of wildland fire emissions across the contiguous United States, *Atmos. Environ.*, *38*(21), 3489–3499.

Liu, Y., J. A. Sarnat, B. A. Coull, P. Koutrakis, and D. J. Jacob (2004a), Validation of multiangle imaging spectroradiometer (MISR) aerosol optical thickness measurements using aerosol robotic network (AERONET) observations over the contiguous United States, *J. Geophys. Res.*, *109*, D06205, doi:10.1029/2003JD003981.

Liu, Y., R. J. Park, D. J. Jacob, Q. B. Li, V. Kilaru, and J. A. Sarnat (2004b), Mapping annual mean ground-level PM2.5 concentrations using Multiangle Imaging Spectroradiometer aerosol optical thickness over the contiguous United States, *J. Geophys. Res.*, *109*, D22206, doi:10.1029/2004JD005025.

Liu, Y., P. Koutrakis, and R. Kahn (2007a), Estimating fine particulate matter component concentrations and size distributions using satellite-retrieved fractional aerosol optical depth: Part 1—Method development, *J. Air Waste Manage. Assoc.*, *57*(11), 1351–1359.

Liu, Y., P. Koutrakis, R. Kahn, S. Turquety, and R. M. Yantosca (2007b), Estimating fine particulate matter component concentrations and size distributions using satellite-retrieved fractional aerosol optical depth: Part 2—A case study, *J. Air Waste Manage. Assoc.*, *57*(11), 1360–1369.

Liu, Y., B. A. Schichtel, and P. Koutrakis (2009), Estimating particle sulfate concentrations using MISR retrieved aerosol properties, *IEEE J. Sel. Top. Appl. Earth Obs. Remote Sens.*, *2*(3), 176–184.

Martin, R. V., D. J. Jacob, R. M. Yantosca, M. Chin, and P. Ginoux (2003), Global and regional decreases in tropospheric oxidants from photochemical effects of aerosols, *J. Geophys. Res.*, *108*(D3), 4097, doi:10.1029/2002JD002622.

Martin, M. V., J. A. Logan, R. A. Kahn, F. Y. Leung, D. L. Nelson, and D. J. Diner (2010), Smoke injection heights from fires in North America: Analysis of 5 years of satellite observations, *Atmos. Chem. Phys.*, *10*(4), 1491–1510.

Martonchik, J. V., D. J. Diner, R. Kahn, B. Gaitley, and B. N. Holben (2004), Comparison of MISR and AERONET aerosol optical depths over desert sites, *Geophys. Res. Lett.*, *31*, L16102, doi:10.1029/2004GL019807.

Olivier, J. G. J., A. F. Bouwman, K. W. Van der Hoek, and J. J. M. Berdowski (1998), Global air emission inventories for anthropogenic sources of NOx, NH3 and N2O in 1990, *Environ. Pollut.*, *102*, 135–148.

Park, R. J., D. J. Jacob, B. D. Field, R. M. Yantosca, and M. Chin (2004), Natural and transboundary pollution influences on sulfate-nitrate-ammonium aerosols in the United States: Implications for policy, *J. Geophys. Res.*, *109*, D15204, doi:10.1029/2003JD004473.

Petrenko, M., R. A. Kahn, M. Chin, A. J. Soja, T. Kucsera, and Harshvardhan (2012), The use of satellite-measured aerosol optical depth to constrain biomass burning emissions source strength in the global model GOCART, *J. Geophys. Res.*, *117*, D18212, doi:10.1029/2012JD017870.

Pope, C. A., M. Ezzati, and D. W. Dockery (2009), Fine-particulate air pollution and life expectancy in the United States, *N. Engl. J. Med.*, *360*(4), 376–386.

Ridley, D. A., C. L. Heald, and B. Ford (2012), North African dust export and deposition: A satellite and model perspective, *J. Geophys. Res.*, *117*, D02202, doi:10.1029/2011JD016794.

Sayer, A. M., G. E. Thomas, P. I. Palmer, and R. G. Grainger (2010), Some implications of sampling choices on comparisons between satellite and model aerosol optical depth fields, *Atmos. Chem. Phys.*, *10*(22), 10,705–10,716.

Veefkind, J. P., K. F. Boersma, J. Wang, T. P. Kurosu, N. Krotkov, K. Chance, and P. F. Levelt (2011), Global satellite analysis of the relation between aerosols and short-lived trace gases, *Atmos. Chem. Phys.*, *11*(3), 1255–1267.

Wang, Y. X., M. B. McElroy, D. J. Jacob, and R. M. Yantosca (2004), A nested grid formulation for chemical transport over Asia: Applications to CO, *J. Geophys. Res.*, *109*, D22307, doi:10.1029/2004JD005237.

Wang, W. T., J. J. Qu, X. J. Hao, Y. Q. Liu, and W. T. Sommers (2007), An improved algorithm for small and cool fire detection using MODIS data: A preliminary study in the southeastern United States, *Remote Sens. Environ.*, *108*(2), 163–170.

Wang, J., S. C. van den Heever, and J. S. Reid (2009), A conceptual model for the link between Central American biomass burning aerosols and severe weather over the south central United States, *Environ. Res. Lett.*, *4*(1), 015003, doi:10.1088/1748-9326/4/1/015003.

Wang, J., X. G. Xu, R. Spurr, Y. X. Wang, and E. Drury (2010), Improved algorithm for MODIS satellite retrievals of aerosol optical thickness over land in dusty atmosphere: Implications for air quality monitoring in China, *Remote Sens. Environ.*, *114*(11), 2575–2583.

Wang, J., X. G. Xu, D. K. Henze, J. Zeng, Q. Ji, S. C. Tsay, and J. P. Huang (2012), Top-down estimate of dust emissions through integration of MODIS and MISR aerosol retrievals with the GEOS-Chem adjoint model, *Geophys. Res. Lett.*, *39*, L08802, doi:10.1029/2012GL051136.

van der Werf, G. R., J. T. Randerson, L. Giglio, G. J. Collatz, M. Mu, P. S. Kasibhatla, D. C. Morton, R. S. DeFries, Y. Jin, and T. T. van Leeuwen (2010), Global fire emissions and the contribution of deforestation, savanna, forest, agricultural, and peat fires (1997–2009), *Atmos. Chem. Phys.*, *10*(23), 11,707–11,735.

van Donkelaar, A., R. V. Martin, M. Brauer, R. Kahn, R. Levy, C. Verduzco, and P. J. Villeneuve (2010), Global estimates of ambient fine particulate matter concentrations from satellite-based aerosol optical depth: Development and application, *Environ. Health Perspect.*, *118*(6), 847–855.

Yu, F., G. Luo, and X. Ma (2012a), Regional and global modeling of aerosol optical properties with a size, composition, and mixing state resolved particle microphysics model, *Atmos. Chem. Phys.*, *12*(13), 5719–5736.

Yu, H. B., L. A. Remer, M. Chin, H. S. Bian, Q. Tan, T. L. Yuan, and Y. Zhang (2012b), Aerosols from overseas rival domestic emissions over North America, *Science*, *337*(6094), 566–569, doi:10.1126/science.1217576.